Improved quantitative evaluation of the fouling potential in spacer-filled membrane filtration channels through a biofouling index based on the relative pressure drop

Huisman, Kees Theo; Franco-Clavijo, Natalia; Vrouwenvelder, Johannes S.; Blankert, Bastiaan

DOI
10.1016/j.memsci.2023.121400

Publication date
2023

Document Version
Final published version

Published in
Journal of Membrane Science

Citation (APA)
Huisman, K. T., Franco-Clavijo, N., Vrouwenvelder, J. S., & Blankert, B. (2023). Improved quantitative evaluation of the fouling potential in spacer-filled membrane filtration channels through a biofouling index based on the relative pressure drop. *Journal of Membrane Science*, *671*, Article 121400. https://doi.org/10.1016/j.memsci.2023.121400

Journal of Membrane Science 671 (2023) 121400

Contents lists available at ScienceDirect

Journal of Membrane Science

journal homepage: www.elsevier.com/locate/memsci

Improved quantitative evaluation of the fouling potential in spacer-filled membrane filtration channels through a biofouling index based on the relative pressure drop

Kees Theo Huisman [a,*], Natalia Franco-Clavijo [a], Johannes S. Vrouwenvelder [a,b,**], Bastiaan Blankert [a]

[a] King Abdullah University of Science and Technology (KAUST), Water Desalination and Reuse Center (WDRC), Biological and Environmental Science and Engineering Division (BESE), Thuwal, 23955-6900, Saudi Arabia
[b] Delft University of Technology, Faculty of Applied Sciences, Department of Biotechnology, Van der Maasweg 9, 2629 HZ, Delft, the Netherlands

ARTICLE INFO

Keywords:
Operational performance
Biofouling
Seawater desalination
Optical coherence tomography
Reverse osmosis

ABSTRACT

In this study, a biofouling index based on the relative pressure drop is presented to quantitatively evaluate the amount of fouling in spacer-filled membrane filtration channels. The biofouling index was defined as the inverse of the time to reach a relative pressure drop of 100% and can be interpreted as a fouling rate or cleaning frequency. The index was applied to evaluate biofilm growth in membrane fouling simulators with reverse osmosis membranes and commercial feed spacers operated with different feed water nutrient concentrations and crossflow velocities. Biofilm accumulation on the membrane and feed spacer was characterized in situ using optical coherence tomography. We showed that the biofouling index is directly related to the volume of biofouling independent of the applied crossflow velocity and a suitable tool for improved quantitative comparison of the biofouling rate. Furthermore our results suggest that the pressure drop is better described as function of the velocity at the perimeter of a spacer cell instead of the average velocity in the channel. Although the biofouling index is developed for biofouling, the index may be applied to quantitatively assess mitigation strategies in spacer filled channels for a wider range of fouling types.

1. Introduction

While freshwater demand is increasing globally, water availability is decreasing due to desertification and the contamination of freshwater resources [1]. Desalination and wastewater reuse are important approaches to fulfill future water demands [1,2]. Spiral wound reverse osmosis and nanofiltration processes have been widely applied for the production of high-quality water from seawater and wastewater. In spiral wound membrane elements, a feed spacer is placed between two membrane sheets to provide structural integrity to the feed channel. When the feed stream contains biodegradable substances, bacteria deposited on the membrane and spacer can grow into biofilms, which are aggregates of cells in a matrix of extracellular polymeric substances adhering to a surface and/or to each other [3]. Excessive formation of biofilms can lead to biofouling, which causes an unacceptable decrease in operational performance and an increase in operating costs [4].

Membrane fouling results in increased transmembrane pressure, salt passage, and feed channel pressure drop, which negatively affect energy consumption, productivity, and water quality, and necessitate corrective actions such as chemical cleaning. The pressure drop is one of the main indicators of operational problems caused by fouling [5]. An excessive pressure drop may result in telescoping, which causes mechanical damage to membrane elements. Therefore, commercial elements should be cleaned when the feed channel pressure drop increases by 10–15% [6], demonstrating the necessity of predicting and controlling the impact of fouling on the pressure drop.

Continuous efforts have been dedicated to controlling the impact of fouling on the feed channel pressure drop and include engineering novel spacers [7-11] and spacer coatings [12,13], developing novel cleaning agents [14,15], optimizing operating conditions such as crossflow

* Corresponding author.
** Corresponding author. King Abdullah University of Science and Technology (KAUST), Water Desalination and Reuse Center (WDRC), Biological and Environmental Science and Engineering Division (BESE), Thuwal, 23955-6900, Saudi Arabia.
E-mail address: kees.huisman@kaust.edu.sa (K.T. Huisman).

https://doi.org/10.1016/j.memsci.2023.121400
Received 28 November 2022; Received in revised form 9 January 2023; Accepted 15 January 2023
Available online 18 January 2023

velocity and permeate flux [16-19], and controlling the feed water composition [5,20,21]. To assess the effectiveness of such mitigation strategies, it is desirable to establish the fouling rate during an experiment and/or the fouling state before and after cleaning. Ideally, this involves a fouling indicator that provides a correct interpretation of the amount of fouling and the impact of fouling on operational performance.

Various representations of the pressure drop are commonly used as a fouling indicator such as the pressure drop [14,22], the pressure drop increase [17,20,23,24], and the relative pressure drop [5,25]. The pressure drop can be expressed as the product of fluid properties, the superficial crossflow velocity, and the feed channel geometry. Fouling is experienced as an increase in pressure drop caused by a change in channel geometry. The channel geometry, fluid properties, and superficial velocity are often intentionally varied between and within experiments. To compare the impact of velocity on fouling, it is necessary to remove the primary dependence of the pressure drop on velocity.

In industrial practice, the relative change in pressure drop is commonly used as a criterion to initiate cleaning [6]. The primary dependence of the pressure drop on fluid properties and velocity may be removed in relative representations of the pressure drop such as the increase in pressure drop divided by the initial pressure drop. However, normalization conducted in this manner can potentially distort the interpretation of fouling data [26]. Thus, the conditions under which a comparison of relative pressure drop data is appropriate must be analyzed.

Relative pressure drop measurements can be compared with optical coherence tomography (OCT) images to validate the link between the biofouling structure and operational performance parameters such as relative pressure drop. OCT offers a non-invasive and independent way to quantify the change in the amount of fouling in the feed channel. In previous studies, qualitative links were established between the pressure drop and various structural parameters including mean fouling thickness, maximum fouling thickness, surface roughness, porosity, macro porosity, and biovolume [22,27-29]. However, a quantitative relation based on the theory of fluid dynamics is desirable for the development of effective mitigation strategies as well as the prediction and modeling of the impact of fouling on operational performance.

Finally, the development of effective mitigation strategies requires the evaluation of numerous experimental conditions. Currently, studies compare curves showing the change in pressure drop [14,17,20,22-24] or relative pressure drop [5,6,25] over time. For improved quantitative comparison of various experimental conditions, it is preferable to have a single number characterizing the fouling situation.

The objective of this study is to establish a robust fouling indicator that quantitatively represents the amount of fouling in spacer-filled channels. We show and discuss how (i) the absolute and relative pressure drop depend on the crossflow velocity, (ii) the relative pressure drop depends on the amount of biofouling through a geometry factor, and (iii) the biofouling index based on the relative pressure drop can be used to compare biofouling under different crossflow velocities. OCT imaging is used to establish the quantitative relations between the geometry of fouled spacer-filled channels and the relative pressure drop. A biofouling index based on the relative pressure drop is presented for quantitative evaluation of biofouling independent of the crossflow velocity.

2. Theoretical background

The operational performance of spiral wound modules for membrane filtration is characterized by the feed channel pressure drop, transmembrane pressure, and solute passage. The pressure drop is typically described by a well-known friction relation [30] based on a characteristic velocity v, a characteristic length, in this case, the hydraulic diameter (d_h), and the Fanning friction factor (f), which is a function of the Reynolds number (Re). The equations are expressed as:

$$DP = \frac{1}{2}\rho \bullet v^2 \bullet f \bullet \frac{L}{d_h} \quad \text{Eqn(1)}$$

$$f = m \bullet Re^{-n} \quad \text{Eqn(2)}$$

$$Re = \rho \bullet v \bullet \frac{d_h}{\eta} \quad \text{Eqn(3)}$$

where ρ is the density of the fluid, L is the channel length, η is the dynamic viscosity, and m and n are experimentally determined constants of the spacer-filled channel.

There are different ways in which the characteristic velocity and characteristic length can be defined. In this study, the superficial velocity is used as a reference and defined as the crossflow velocity in an empty channel. Other useful definitions of the velocity are the average velocity and the perimeter velocity. It should be noted that neither of these definitions of velocities take into account that the flow may change direction. A spacer consists of many cells, where water has to pass from cell to cell around the spacer filaments. The average velocity is defined as the superficial velocity divided by the channel porosity $\varepsilon_{channel}$, i.e. the total void fraction of a spacer cell (Eqn. (4), (Schock and Miquel [31]). The perimeter velocity occurs at the spacer filaments, where the void fraction available for water flow is the smallest. The perimeter velocity is defined as the superficial velocity divided by the perimeter porosity ε_{per} (Eqn. (5)), i.e., the void fraction at the transition between spacer cells as shown in Fig. 1. The perimeter porosity decreases by the development of fouling at the transition between spacer cells.

Hydraulic losses are broadly categorized into so called major losses, due to friction and minor losses, due to changes in the fluid velocity [30]. The characteristic relation as proposed by Schock and Miquel [31] is consistent with the assumption that friction is the main cause of pressure loss. Conversely, if the minor losses are dominant, it may be expected that the pressure loss is proportional to the squared change in velocity, which is roughly proportional to the perimeter velocity.

$$v_{avg} = \frac{v_s}{\varepsilon_{channel}} \quad \text{Eqn(4)}$$

$$v_{per} = \frac{v_s}{\varepsilon_{per}} \quad \text{Eqn(5)}$$

2.1. Representations of the feed channel pressure drop

The superficial velocity is often intentionally varied between and within experiments. The impact of superficial velocity on the pressure drop is twofold. The superficial velocity (i) directly affects the pressure drop due to a change in the friction and (ii) indirectly affects the pressure drop due to a change in fouling development which impacts the channel geometry (Eqn. (1)). To evaluate the impact of velocity on the fouling development it is necessary to remove the primary dependence of the pressure drop on the velocity. In this section, we show that the relative pressure drop (RPD, Eqn. (6)) removes the primary dependence on velocity.

$$RPD = \frac{DP_t - DP_0}{DP_0} \bullet 100\% \quad \text{Eqn(6)}$$

Normalization can potentially alter the way fouling data are interpreted [26]; therefore, we evaluate under what conditions it can be justified to compare different experiments based on the RPD. When Eqns. (2)–(5) are inserted into Eqn. (1), it follows that the pressure drop depends on the fluid properties (ρ and η), superficial velocity, characteristic constants of the spacer-filled channel (m, n), and a geometry factor g:

$$PD = \frac{1}{2} m \bullet \rho^{1-n} \bullet \eta^n \bullet v_s^{2-n} \bullet g \quad \text{Eqn(7)}$$

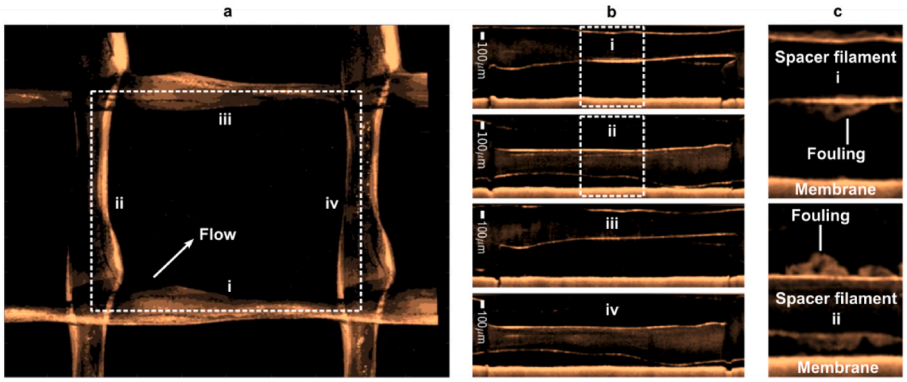

Fig. 1. OCT images of a pristine spacer cell showing the concept of perimeter porosity. **a** Top view of the spacer cell showing the four filaments that form the transition between spacer cells, i.e. the perimeter **b** Cross-sections of the four spacer filaments that form the perimeter. The perimeter porosity is the narrowest void fraction at the transition between spacer cells. **c** Fouling on the spacer filaments and the membrane surface near the spacer filaments decreases the perimeter porosity.

here, the geometry factor is defined as:

$$g = L \bullet \frac{\varepsilon^{-2+n}}{d_h^{1+n}} \qquad \text{Eqn(8)}$$

where the expression for channel porosity ε can be ε_{avg} or ε_{min} depending on which definition is used for the velocity.

The RPD removes the primary dependence of pressure drop on velocity if the exponent n does not change upon fouling. Schock and Miquel [31] found that the exponent is the same for many feed spacer geometries. If it is assumed that the characteristic constant of the spacer-filled channel n does not change upon fouling, the relative pressure drop can be a suitable indicator to compare the impact of superficial velocity on the amount of biofouling. When PD_0 and PD_t are measured at the same velocity ($v_A(0) = v_A(t)$), the RPD can be calculated. Given that the specific density, dynamic viscosity, and channel length are constant and independent of fouling, the RPD increase from time t_0 to t_t depends only on the geometric properties:

$$RPD = \frac{g_t - g_0}{g_0} \bullet 100\% = \left(\left(\frac{\varepsilon_0}{\varepsilon_t} \right)^{2-n} \bullet \left(\frac{d_{h_0}}{d_{h_t}} \right)^{1+n} - 1 \right) \bullet 100\% \qquad \text{Eqn(9)}$$

Since the velocity cancels out of the RPD, experiments with different velocities and similar geometry can be compared ($v_A \neq v_B$), providing that the RPD is calculated for the same velocity ($v_A(0) = v_A(t)$).

2.2. Biofouling index

To represent the outcome of a fouling experiment, by monitoring the RPD over time, we define a biofouling index with a single number as the inverse of the time t^* required to reach a certain RPD (Eqn. (10)). In this way, a higher biofouling index (BFI) intuitively corresponds to a higher fouling rate.

$$BFI = \frac{1}{t^*} \qquad \text{Eqn(10)}$$

In this study, we choose a biofouling index as the inverse of the time t^* required to reach a RPD of 100%. For large-scale systems, it is typically recommended to initiate corrective cleaning when the relative pressure drop increases by 15% [6]. Such systems typically have 7–8 membrane elements of 1-m length in series, while biofouling predominantly occurs in the lead element [32-34]. In the case when all biofouling occurs in the lead element, an increase in the relative pressure drop of the vessel of 15% would correspond to a 105%–120% increase in the relative pressure drop of the lead vessel with 7 or 8 elements respectively. Thus, given that part of the fouling will occur in downstream elements, we estimate that a 15% increase over an entire pressure vessel corresponds to an approximately 100% increase over the lead element.

3. Materials and methods

3.1. Setup

Membrane fouling simulators were used in this experiment. The simulators represent spiral wound RO and NF modules in terms of the membrane and spacer materials, the hydrodynamic conditions, permeate flux, and feed channel pressure drop development upon fouling [32,35]. The membrane fouling simulators had an effective membrane length of 0.2 m and a width of 0.04 m. The height of the feed channel was determined by the feed spacer. The simulator, based on the design from Vrouwenvelder et al. [32], consisted of two aluminum plates with connectors for feed, concentrate, and permeate flow and for pressure drop measurements. One aluminum plate had an optical window that enabled in-situ visualization of biofouling on the membrane, the spacer, and the optical window of the feed channel with OCT. A schematic of the setup is presented in Fig. 1.

Local tap water from seawater reverse osmosis was filtered using a sediment and granular activated carbon two-step filtration cartridge (AC–SC–10-NL, Bluefilters, Germany) to remove residual chlorine before feeding to the simulator [36]. The filtered water which contained typical ions such as calcium and sodium, was enriched with nutrients dosed from a 10-L concentrated stock solution and fed to the simulator. The superficial velocity set point v_{sp} was maintained by a feed water pump (EW-07002-25, Cole-Parmer, USA) coupled with a mass flow transmitter and controller (mini CORI-FLOW™ M15, Bronkhorst, Netherlands). The nutrient dosing set point C_{sp} was achieved by a dosing pump (D Series, Tuthill, USA) coupled with a mass flow transmitter and controller (mini CORI-FLOW™ M15, Bronkhorst, Netherlands). The permeate flux set point J_{sp} was maintained by regulating the concentrate pressure with a pressure controller (IN-PRESS P502CI, Bronkhorst, Netherlands) coupled with a mass flow meter (mini CORI-FLOW™ M14, Bronkhorst, Netherlands). The pressure drop across the feed channel was monitored by a differential pressure transmitter (Deltabar PMD75, Endress + Hauser, Switzerland).

3.2. Membrane and spacer

Nanofiltration membrane sheets (FilmTec NF90, DuPont, USA), feed spacers (nominal thickness: 34 mil), and permeate spacers were obtained from virgin commercial spiral wound membrane modules. The membranes were placed in membrane fouling simulators with the active layer facing the feed solution and the spacers were placed at an angle of

approximately 45° between the filaments and the flow direction of the feed.

3.3. Biofilm growth

Membranes were conditioned with filtered tap water at a flow rate of 0.16 m/s, representative for practice [20,37], for 7 days prior to the fouling experiment. At the end of the conditioning phase, the relationship between the fluid superficial velocity and pressure drop in a clean feed channel was characterized by decreasing the velocity stepwise form 0.16 m/s to 0.04 m/s in steps of 0.02 m/s. Subsequently, the velocity was adjusted to the desired velocity set point to start the fouling experiment in which the filtered tap water was enriched with nutrients dosed from a 10-L concentrated stock solution. The stock solution consisted of sodium acetate (S7670, Sigma Aldrich, USA), sodium nitrate (71755, Sigma Aldrich, USA), and sodium phosphate (71500, Sigma Aldrich, USA) dissolved in ultrapure water at a mass ratio C:N:P of 100:20:10. To avoid bacterial growth in the stock solution, the pH was adjusted to 11 by the addition of sodium hydroxide (S5881, Sigma Aldrich, USA). The high pH of the stock solution did not affect the pH of the feed solution because the dosage flow rate was small compared with the feed flow rate. Table 1 shows the nutrient and operating conditions. At the end of fouling experiment 1 in Table 1, the relationship between the superficial velocity and pressure drop in the fouled feed channel was characterized again by decreasing the velocity stepwise. By decreasing the velocity, we aimed to prevent removal of biofilm by shear forces.

3.4. OCT imaging

The development of biofilms was monitored by an OCT system (GAN610C1, Thorlabs GmbH, Germany) with a central light source wavelength of 930 nm. The system was configured to image with a refractive index of 1.33 at an A-scan rate of 36 kHz. To flatten the noise floor and improve image quality, an A-scan averaging of 20 was applied. OCT images were obtained at the same location selected a priori. The volumetric images had a resolution of 499 × 499 × 558 voxels and a field of view of 5.0 mm × 5.0 mm × 1.2 mm. The processing and analysis of images with respect to the biofilm volume fraction, channel height, and channel porosity was conducted with a custom Matlab® (MathWorks, USA) script with a method based on Fortunato et al. [38].

4. Results

In the first part of this study, the dependence of the relative pressure drop on the superficial velocity is evaluated. In the second part, the impact of feed channel geometry on the RPD is evaluated. In the third part, a biofouling index based on the RPD is presented and it is shown how the biofouling index facilitates the comparison of biofouling under different nutrient concentrations and crossflow velocities.

Table 1
Nutrient and operating conditions tested in this study. The operating conditions v_{sp}, C_{sp}, and J_{sp}, refer to the set points of the superficial crossflow velocity, nutrient dosing, and permeate flux, respectively. Concentrations of carbon (C), nitrogen (N), and phosphorus (P) refer to the concentrations in the enriched feed water.

Experiment number (−)	v_{SP} (m/s)	C_{SP} (mL/h)	J_{SP} (L/m^2/h)	C (μg/L)	N (μg/L)	P (μg/L)	Section (−)
1	0.16	30	20	200	40	20	4.1
2–7	0.16	30	7.5	200	40	20	4.2
8–9	0.04	30	20	200	40	20	4.3
10–11	0.08	30	20	100	20	10	4.3
12–13	0.08	30	20	200	40	20	4.3
14–15	0.16	30	20	50	10	5	4.3
16–17	0.16	30	20	100	20	10	4.3
18–21	0.16	30	20	200	40	20	4.3
22–23	0.16	30	20	25	5	2.5	4.3
24–25	0.16	30	20	300	60	30	4.3

4.1. Impact of velocity on the relative pressure drop

We investigated whether the relative pressure drop may be used to compare parallel experiments with different velocities (see Table 1, experiment 1for details). The concept of the RPD is shown in Fig. 2. Fig. 2a shows how the RPD is determined from the exponential part of the pressure drop curve during the fouling experiment. The RPD is defined as the increase in pressure drop divided by the initial pressure drop; thus, a doubling of the pressure drop corresponds to a 100% increase in the RPD. Fig. 2b shows the RPD during the fouling experiment together with the biofilm volume fraction derived from the OCT images. The change in RPD matched well with the change in biofilm volume fraction.

The superficial crossflow velocity was decreased stepwise at the end of the experiment when the RPD was approximately 380%. By decreasing the velocity, we aimed to prevent removal of biofilm by shear forces. The resulting relation between the velocity and pressure drop of the clean channel and fouled channel is plotted in Fig. 4a. The same biofilm resulted in a different pressure drop depending on the superficial crossflow velocity. For a specific channel geometry, the measured pressure drop values lie on a curve according to:

$$PD = a \bullet v_s^{2-n} \quad \text{Eqn(11)}$$

here, a and n are fitting parameters. If the fitting parameter n does not change upon fouling, the velocity cancels out of the RPD, resulting in Eqn. (9). In this study, n was invariant between the clean and fouled channel (0.41 ± 0.02), suggesting that the RPD was independent of the applied velocity. This is further confirmed by Fig. 4b, which depicts the effect of the decrease in velocity on the RPD and the biofilm volume fraction of the fouled channel. A minor velocity dependency of both the RPD and biofilm volume fraction can be observed. However, the correlation between the superficial crossflow velocity and biofilm volume was not statistically significant (correlation coefficient: 0.26 and p-value: 0.57). Furthermore, the OCT images shown in Fig. 5 confirm that during the velocity changes, the biofilm morphology was not affected. The observed increase in RPD at lower velocities may be caused by the increased error margins of the pressure drop transmitter at lower velocities. With decreasing velocity, the maximum measurement error of the pressure drop transmitter (1 mbar) became larger compared with the measured value of the pressure drop. This measurement error propagated through the calculation of the relative pressure drop, resulting in increasing error margins at lower velocities. Thus, the same biofilm results in the same relative pressure drop independent of the superficial crossflow velocity.

4.2. Impact of feed channel geometry on the relative pressure drop

We examined whether minor geometric differences in replicate flow channels affect the impact of biofilm on the relative pressure drop. The initial channel geometry of replicate flow cells can deviate from product specifications due to imprecisions in the manufacturing process of the feed spacers and flow cells. The RPD is dependent on the initial channel geometry. Thus, it should be assessed whether small variations in the initial geometry have a significant impact on the RPD.

We compared six replicate membrane fouling simulator setups containing different pieces of one type of spacer under identical operational conditions (see Table 1, experiments 2–7 for details). The initial geometry is a function of the channel porosity and the hydraulic diameter, which is a function of the feed channel height and the filament diameter and length. From the OCT images, small differences were observed in the initial porosity, height, and filament diameter between the feed

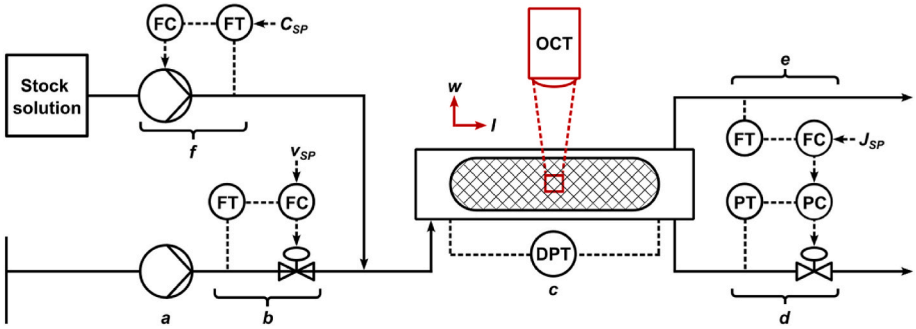

Fig. 2. Experimental setup for operation with a constant feed flow and permeate flux. The set points v_{sp}, C_{sp}, and J_{sp}, refer to the superficial crossflow velocity, nutrient dosing, and permeate flux, respectively. **a** Feed water pump; **b** Mass flow transmitter and controller; **c** Differential pressure transmitter; **d** Pressure transmitter and controller; **e** Mass flow transmitter and controller; **f** Dosing pump.

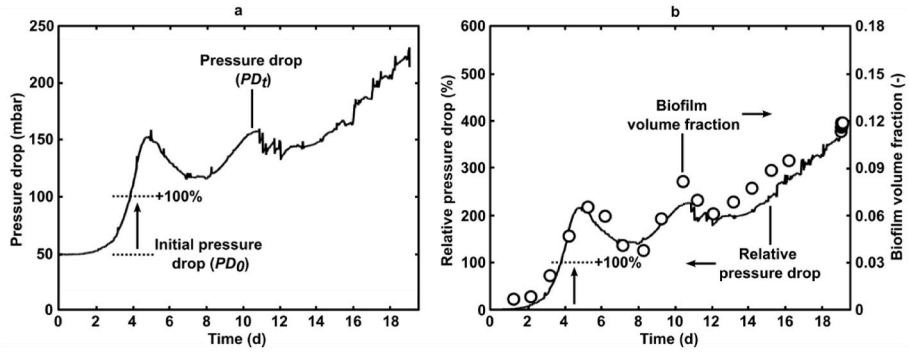

Fig. 3. Pressure drop, relative pressure drop, and biofilm volume fraction as a function of time. **a** Pressure drop as a function of time (PD_t). The horizontal dashed lines indicate the initial pressure drop (PD_0) and an increase of 100% compared with the initial pressure drop. **b** Relative pressure drop (line) and biofilm volume fraction (circles) as a function of time. The biofilm volume fraction was determined from the OCT images. The figure shows good agreement with the relative pressure drop and the biofilm volume fraction.

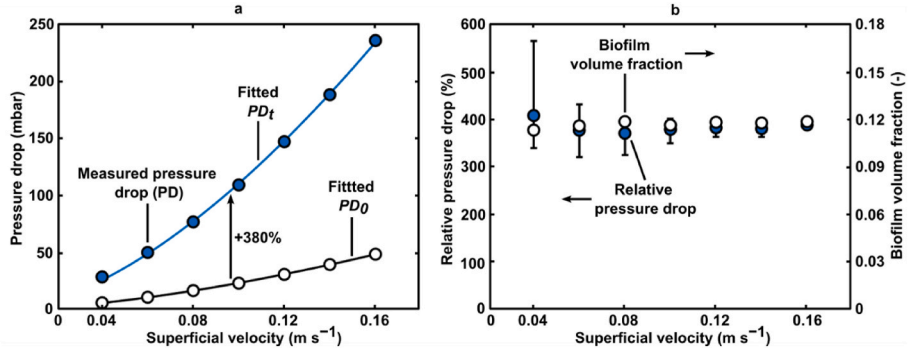

Fig. 4. Pressure drop, relative pressure drop (RPD), and biofilm volume fraction as a function of superficial crossflow velocity. The figure corresponds to the initial and final point of the fouling state in Fig. 3 **a** Pressure drop (PD) in the feed channel as a function of superficial crossflow velocity for a clean channel (PD_0) and a fouled channel (PD_t). In the fouled channel, the velocity was decreased to avoid detachment of the biofilm due to shear forces. The same biofilm results in a different pressure drop depending on the superficial crossflow velocity according to $PD = a \bullet v_s^{2-n}$ shown by the solid lines. The n is identical for both the clean and fouled channels (0.41 ± 0.02). **b** Relative pressure drop and biofilm volume fraction as a function of superficial crossflow velocity. The biofilm volume fraction was determined from the OCT images and shows that the volume fraction was not affected by the change in velocity. The RPD data show that the same biofilm results in the same relative pressure drop at different velocities.

channels of the six fouling simulators (Table 2).

We further investigated the reproducibility of the relative pressure drop measurements by plotting the relative pressure drop as a function of the biofilm volume fraction in Fig. 6a. A strong correlation between the RPD and the biofilm volume fraction was observed (correlation coefficient: 0.98 and confidence: >99.5%). Thus, the RPD was not affected by the minor variations in the initial channel geometry and is a good indicator of the amount of biofilm in a flow channel.

When the relative pressure drop was zero, i.e., in the clean channel, the biofilm volume fraction ranged from 0 to 0.004 ± 0.009, while a biofilm volume fraction of 0 was expected. Our OCT image analysis algorithm quantifies the biofilm by counting the voxels with a signal above a threshold, which were below the threshold in the initial image. Voxels that belong to the membrane or spacer that were not visible in the initial image but were visible in a later image contribute to the observed biofilm volume, thus introducing a measurement error (0.009) in addition to a bias towards measuring a too high biofilm volume (0.004). Consequently, the quantification of small volumes of biofilm from the OCT images was challenging.

We observed in Fig. 6 that a notably small amount of biofilm of approximately 4% of the flow channel volume can result in a significant increase in relative pressure drop of about 100%. This observation challenges the prevailing idea that the pressure drop depends on the average crossflow velocity and the corresponding RPD depends on the channel porosity and hydraulic diameter [9,31,39-41] because these properties are hardly affected. Alternatively, it can be argued that the PD depends on the perimeter velocity which occurs at the spacer filaments, where the void fraction available for water flow is the smallest, and the corresponding RPD depends on the perimeter porosity and hydraulic diameter. Therefore, we evaluated to what degree a strong increase in

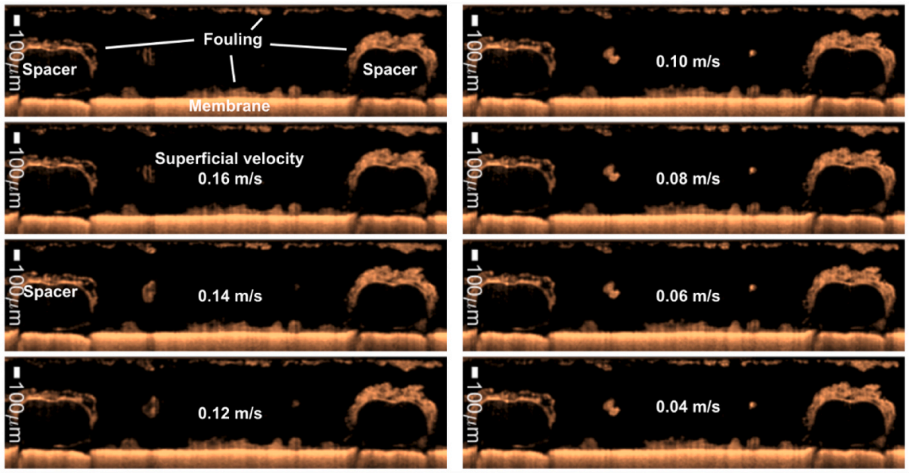

Fig. 5. Cross-sections selected from 3D OCT images of a fouled feed channel at an RPD of approximately 380% at different superficial crossflow velocities. The figure corresponds to the biofilm volume fraction in Fig. 4b. The velocity was decreased to prevent detachment of the biofilm due to shear forces. The biofouling morphology was not affected by the change in the velocity.

Table 2
Small differences were observed in the channel geometry of replicate membrane fouling simulators (MFS). The channel height H_{OCT} and porosity of the clean channel $\varepsilon_{channel}$ were obtained from the OCT images. H_{OCT} is the difference between the maximum signal corresponding to the membrane and the glass in the OCT images and did not precisely correspond to the actual height of the channel. The estimator of the actual height $\widehat{H}$ was calculated by scaling the mean of H_{OCT} to the theoretical height of a feed spacer with a thickness of 34 mil (863 μm). $\widehat{d}_{f_0}$ and $\widehat{d}_{h_0}$ are estimations of the diameter of the spacer filament and the hydraulic diameter of the clean channel, respectively.

MFS	H_{OCT}	ε_{avg_0}	$\widehat{H}$	$\widehat{d}_f$	$\widehat{d}_h$
(−)	(μm)	(−)	(μm)	(μm)	(μm)
1	1021	0.883	894	447	1147
2	946	0.891	827	414	1029
3	956	0.890	836	418	1036
4	1053	0.887	921	461	1093
5	982	0.890	859	430	1052
6	961	0.892	841	421	1039
μ_{all}	987	0.889	863	432	1054
σ_{all}	42	0.003	37	18	25

the PD would be explained by a change in biofilm volume fraction in case the PD depends on the average velocity and on the perimeter velocity.

Fig. 7 shows the theoretical PD as a function of the biofilm volume fraction if PD depends on the average velocity and on the perimeter velocity. The OCT images in Fig. 6b shows that in the different membrane fouling simulators the biofilm was mainly located around the spacer. Hence, for theoretical calculations it was assumed that all fouling was located around the spacer, forming a growing cylinder. From Fig. 7 it is evident that the impact of biofilm volume on the pressure drop is significantly larger for PD dependence on perimeter velocity instead of average velocity.

Subsequently, the measured PD (measurement accuracy 1 mbar) and biofilm volume fraction (measurement accuracy 0.009) were compared with the theoretical lines. A strong mismatch was observed between the measurements and the theoretical line if the PD depends on average velocity. The mismatch increases with increasing biofilm volume fraction. The mismatch was considerably smaller between the measurements and the theoretical line if the PD depends on the perimeter velocity, suggesting that the pressure drop may be better described as a function of the perimeter velocity instead of the average velocity, and that the relative pressure drop may be better described as a function of the perimeter porosity instead of the channel porosity.

4.3. The biofouling index based on the relative pressure drop to evaluate fouling potential

We utilized the biofouling index based on the relative pressure drop to compare biofilm development for different operating conditions including different superficial crossflow velocities (see Table 1, experiment 8–25 for details). The biofouling index is the inverse of the time to reach a relative pressure drop of 100%, as shown in Fig. 2b. The index represents a biofouling rate, i.e., the difference between the growth and detachment rate, and can be loosely interpreted as the required cleaning frequency.

Typically, the impact of a variable of interest on biofilm formation is shown by a number of pressure drop curves. Fig. 8a depicts such curves for the impact of nutrient concentration, showing that with increasing nutrient concentration, the pressure drop increases more rapidly. However, it is difficult to quantify the impact of nutrient concentration on the pressure drop based on this plot. From the same data, the biofilm index can be calculated as presented in Fig. 8c. A Monod curve $BFI = \mu_{max} \bullet \frac{C}{C+K}$ was fitted to the datapoints using the lsqcurvefit function in Matlab® where C is the nutrient concentration, and the two fit parameters are the maximum growth rate μ_{max} and the half-velocity constant K. The biofilm index shows that the Monod kinetics provide a good description of biofouling as a function of nutrient concentration. The fouling rate stabilizes at a nutrient concentration higher than approximately 330 μg C/L, indicating that above this concentration, biofilm development was growth-rate limited.

The impact of the superficial crossflow velocity on the pressure drop is shown in Fig. 8b. The biofilm development appears to be faster at higher velocities. However, the same biofilm geometry has a stronger impact on the pressure drop at higher velocities as shown in Fig. 3a because the pressure drop depends on the velocity (Eqn. (11), Fig. 3a). Thus, the pressure drop is unsuitable to compare biofouling at different superficial velocities. Alternatively, the relative pressure drop removes the primary dependence on velocity and is solely a function of the channel geometry (eqn. (9) and Fig. 3b). Consequently, the biofouling index based on the relative pressure drop is solely a function of the channel geometry, where biofilm development is experienced as a change in channel geometry. Therefore, the biofouling index can be used to independently of the velocity compare the amount of fouling in a spacer-filled channel. The change in the biofouling index as function of superficial velocity in Fig. 8d is small compared with the spread in

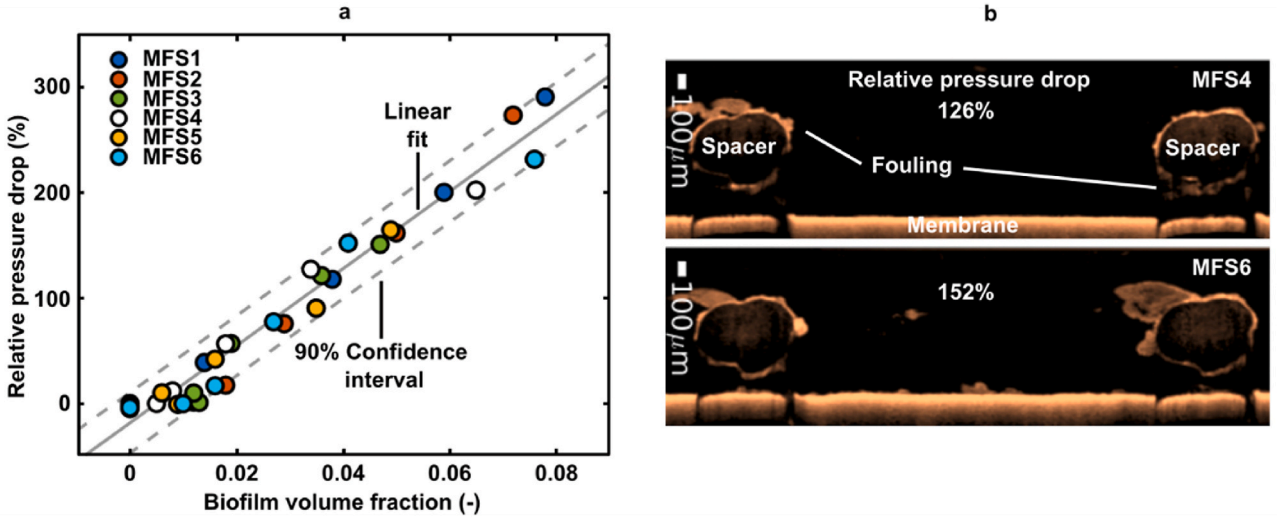

Fig. 6. Relative pressure drop as a function of biofilm volume fraction. The biofilm volume fraction was determined from daily OCT images. **a** Relative pressure drop as a function of biofilm volume fraction in six membrane fouling simulators (MFS). The linear fit and confidence interval were obtained by the Matlab® polyconf function. From the fit, we estimate that there is a small bias in the biofilm volume fraction of 0.004 and an accuracy of 0.009. There is good agreement between the linear fit and the data points, indicating that the relative pressure drop is proportional to the volume of biofilm. **b** Cross-sections selected from 3D OCT images of MFS4 and MFS6 in Fig. 6a at a relative pressure drop of 126% and 152% respectively. In all fouling simulators, biofilm was mainly located around the spacer. At higher pressure drop some biofilm was present on the membrane surface.

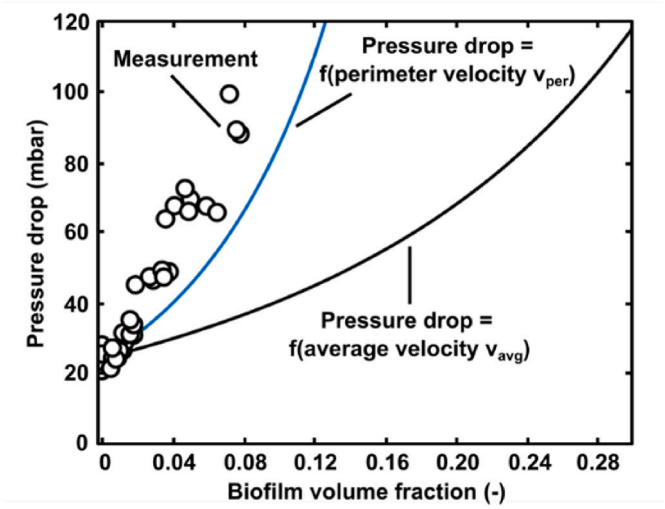

Fig. 7. Relation between pressure drop and biofilm volume fraction. The solid black line and blue line represent the theoretical relation between pressure drop and biofilm volume fraction if the pressure drop depends on the average velocity and the perimeter velocity respectively when biofilm develops on the spacer, forming a growing cylinder. The circles represent the measured relation between the pressure drop and the biofilm volume fraction obtained from OCT images. A better match was observed between the measurements and the theoretical relation between pressure drop and biofilm volume fraction if the pressure drop depends on the perimeter velocity instead of the average velocity. (For interpretation of the references to colour in this figure legend, the reader is referred to the Web version of this article.)

datapoints. The spread in the datapoints potentially originates from seasonal variation in the quality and temperature of filtered local tap water. As a result, no assumptions can be made on the nature of the relation between crossflow velocity and biofouling e.g., linear or exponential. However, the datapoints suggest that a larger superficial crossflow velocity leads to a statistically insignificant reduction in fouling rate.

5. Discussion

5.1. The relative pressure drop independently of velocity represents the amount of fouling

We showed that in a membrane fouling simulator with feed spacers, the same fouling layer resulted in the same relative pressure drop at different superficial crossflow velocities. The pressure drop depends on the velocity ($\sim v_s^{2-n}$), and this exponent was the same for the clean and fouled channel, indicating that only the change in geometry affected the RPD. We believe that this observation is generally applicable to spacer-filled channels in flow cells because in these systems, the pressure drop is predominantly determined by the spacer. Biofouling initially develops on the spacer and membrane surface around the spacer filaments and nodes [5,22,42]. At a relative pressure drop higher than >200% significant area of the membrane surface was covered with fouling. In the current study, we observed similar biofilm development with fouling largely located around the spacer at an RPD of 126% and 152% (Fig. 6b) and significant membrane coverage at an RPD of approximately 380% (Fig. 5.). The membrane could affect the ratio between fouling on the membrane and fouling around the spacer. However, we do not believe there are other commercial membranes that are substantially more prone to fouling than the FilmTec NF90.

Some studies have observed differences in the dependence of the pressure drop on the velocity for a variety of spacer geometries [40,43]. It is plausible that in some fouling situations where biofouling strongly alters the channel geometry, the dependence of the pressure drop on velocity changes because of fouling. In this case, the same amount of fouling could result in a different RPD depending on the velocity. However, since a small amount of fouling results in an operationally relevant RPD increase, we consider that the RPD represents the amount of fouling under typical operating conditions. Nevertheless, we recommend verifying the relation between the pressure drop and superficial crossflow velocity for individual experiments in which it may be expected that the geometry will be significantly altered by the fouling.

5.2. The pressure drop is better described as function of the perimeter velocity instead of the average velocity

In this study, the relative pressure drop linearly depended on the

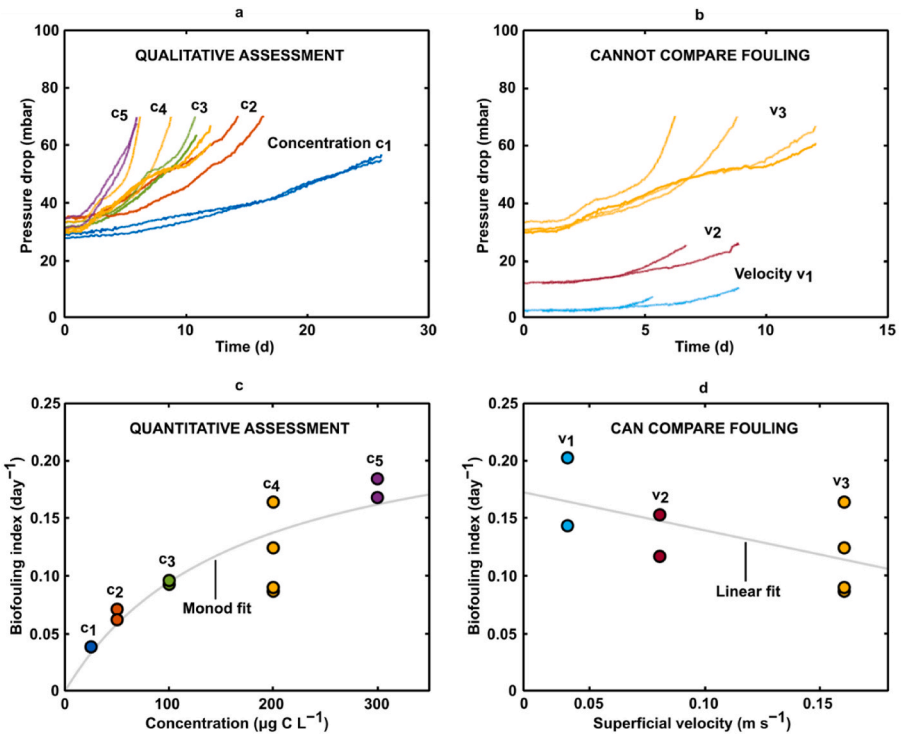

Fig. 8. Biofouling index to evaluate the effect of nutrient concentration and superficial crossflow velocity. **a** Pressure drop data as a function of time for different nutrient concentrations. Fouling is more rapid at higher concentrations but challenging to quantitatively assess. **b** Pressure drop data as a function of time for different velocities. Due to the primary dependence of pressure drop on velocity (Eqn. (11), Fig. 3a), it is not possible to compare the amount of fouling. **c** Biofouling index as a function of concentration obtained from panel a. By plotting the biofouling index, a quantitative relation between biofouling and concentration is revealed. **d** Biofouling index as a function of velocity obtained from panel b. The biofouling index based on the relative pressure drop is solely a function of the channel geometry which changes due to fouling (eqn. (9) and Fig. 3b). Hence, the biofouling index enables the amount of fouling at different velocities to be compared.

biofilm volume fraction in replicate membrane fouling simulators. In all replicates, a small amount of fouling caused a large increase in the RPD. Fouling was mainly situated around the spacer filaments, indicating that fouling on the spacer strongly affects the feed channel pressure drop. Our results suggested that the pressure drop may be better described as a function of the velocity at the perimeter instead of the average velocity and that the relative pressure drop may be better described as a function of the perimeter porosity instead of the channel porosity. Similarly, another experimental study observed that the spacer perimeter, where the velocity is maximum, was the main contributor to the increase in feed channel pressure drop [42]. Previous CFD studies also observed that the pressure drop in a spacer-filled channel is mainly originating at the spacer filaments. In a modeling study of spacer-filled ultrafiltration channels by Da Costa et al. [40] the contribution of different components of the pressure drop was evaluated. It was found that the spacer had major impact on the pressure drop through fluid force on the spacer (form drag) and kinetic losses due to directional flow change, whereas friction at the channel walls contributed marginally to the pressure drop. Ranade and Kumar [44] also identified spacer filaments as main contributor to the pressure drop. In CFD studies of fouled membrane filtration channels it was observed that biofouling on the spacer filaments has significant stronger impact on the pressure drop than biofouling on the membrane by further decreasing the small flow section at the spacer filaments that is the perimeter porosity [45,46]. “Consequently, more effort should be invested in developing effective methods to prevent and clean biofouling near the spacer filaments. Moreover, the realization that the perimeter velocity is an important factor to consider for the pressure drop could be helpful in designing novel feed spacers. Finally, studies on fouling in spacer-filled channels often involve structural analysis of fouling from OCT images in the center of the spacer cell, ignoring possible fouling around the spacer [7,8,10,47–50]. According to our findings, fouling around the spacer should be included when analyzing the impact of modified spacers on biofouling and feed channel pressure drop.

In the current study, the measured relation between biofilm volume fraction and pressure drop was compared with the theoretical relation if the biofilm was located around the spacer, forming a growing cylinder. In practice, the spacer filaments and the biofilm, which is a heterogeneous structure, may deviate from a perfect cylindrical shape. To further increase our understand of the relation between biofouling structure, pressure drop, and relative pressure drop, it is recommended to use CFD simulation using 3D scans of the fouled spacer-filled feed channel generated with OCT.

5.3. A fouling index based on the relative pressure drop enables direct quantitative evaluation of biofouling

A biofouling index was defined as inverse of the time t* required to reach a certain RPD (Eqn. (10)). In this study, time t* was chosen as the time to reach a relative pressure drop of 100% [52,53].Biofilm development can be described by an exponential phase with fast development of biofilm, followed by a quasi-steady-state with fluctuation in the biofilm volume as shown in Fig. 2a [4,54]. Biofilm development during the exponential phase can be described by an exponential curve which is shifted in time by a different time constant to fit different growth curves. Regardless of the choice of the biofouling index such as an RPD bigger or smaller than 100%, the ratio between the time t* for different growth curves is constant in the exponential phase. A biofouling index based on a relative pressure drop larger than 100% may be useful to represent extreme fouling conditions, for example when a membrane element is cleaned less frequently than advised by industry standards. However, during the quasi-steady-state, variations in the relative pressure drop may occur. Therefore, it is recommended that the biofouling index is determined in the exponential phase of the relative pressure drop curve as shown in Fig. 2a.

We showed that the biofouling index based on the RPD can be a suitable tool to evaluate biofilm development for different nutrient concentrations and superficial crossflow velocities. We observed a strong impact of concentration on the biofouling rate, in accordance with previous studies [17,20,23]. Additionally, by plotting the biofouling index versus the nutrient concentration, we found that a Monod relation provides a good description of the impact of nutrient concentration on biofouling. This paves the way toward the accurate prediction of the biofouling rate for a given bulk nutrient concentration,

which can be useful in simulations where the biofouling rate is typically estimated from bacteria growth rates in different systems [46,51,55,56].

Our results suggest that an increase in the superficial crossflow velocity leads to a statistically insignificant decrease in the fouling rate. The impact of velocity is twofold affecting: (i) the hydrodynamic shear acting on the biofilm, which impacts the mechanical stability and the detachment rate of the biofilm [57,58] and (ii) the thickness of the mass transfer boundary layer, which influences the transport of nutrients towards the membrane and biofilm surface [58-60]. Upon increasing the velocity, the thickness of the mass transport boundary layer is decreased, leading to reduced diffusional resistance [61]. On the one hand, the decreased diffusional resistance may reduce the growth rate due to a decline in concentration polarization of solutes. On the other hand, the growth rate may be increased due to an increased flux of solute towards the biofilm. The biofouling rate is the difference between the growth and detachment rate. In our study, the biofouling rate decreased with increasing velocity, indicating that the impact of increased solute flux was smaller than the impact of increased shear and decreased concentration polarization. This finding is supported by a modeling study by Radu et al. [46] and by two experimental studies [16,62]. Other studies reported an increase in biofouling rate with increasing crossflow velocity [17,20,23]. It should be noted that the fouling indicators in other studies were absolute representations of the feed channel pressure drop, the transmembrane pressure, and biomass on the membrane area. These indicators do not always provide a direct measure of the volume of biofilm in the feed channel. Therefore, we recommend using the biofouling index as a parameter for the quantitative evaluation of the biofouling rate and cleaning demand.

6. Conclusion

In this study, a biofouling index was presented based on the time required to reach a 100% increase in relative pressure drop. In membrane fouling simulators with permeation, we evaluated (i) the dependence of pressure drop and relative pressure drop on crossflow velocity, (ii) the impact of changes in feed channel geometry on the relative pressure drop, and (ii) the impact of nutrient concentration and crossflow velocity on the biofouling index. Our conclusions are as follows:

- The pressure drop is better described as function of the velocity at the perimeter of the spacer cells instead of the average velocity, meaning that the relative pressure drop is better described by a function of the perimeter porosity instead of the channel porosity.
- The relative pressure drop measures independently of the applied crossflow velocity the amount of fouling in a spacer-filled channel.
- The relative pressure drop is not affected by minor differences in the initial channel geometry of replicator flow cells.
- The biofouling index based on the relative pressure drop is a suitable parameter for the quantitative evaluation of the biofouling rate and cleaning demand.

Author statement

Kees Theo Huisman: Conceptualization; Methodology; Software; Validation; Formal analysis; Investigation; Data Curation; Writing - Original Draft; Visualization, Natalia Franco-Clavijo: Investigation; Data Curation, Johannes S. Vrouwenvelder: Conceptualization; Methodology; Supervision; Writing - Review & Editing, Bastiaan Blankert: Conceptualization; Methodology; Software; Validation; Supervision; Writing - Review & Editing.

Declaration of competing interest

The authors declare that they have no known competing financial interests or personal relationships that could have appeared to influence the work reported in this paper.

Data availability

Data will be made available on request.

Acknowledgments

The research reported in this publication was supported by funding from King Abdullah University of Science and Technology (KAUST).

References

[1] M. Elimelech, W.A. Phillip, The future of seawater desalination: energy, technology, and the environment, Science 333 (6043) (2011) 712–717, https://doi.org/10.1126/science.1200488.
[2] M.A. Shannon, P.W. Bohn, M. Elimelech, J.G. Georgiadis, B.J. Mariñas, A. M. Mayes, Science and technology for water purification in the coming decades, Nature 452 (7185) (2008) 301–310, https://doi.org/10.1038/nature06599.
[3] M. Vert, Y. Doi, K.-H. Hellwich, M. Hess, P. Hodge, P. Kubisa, M. Rinaudo, F. Schué, Terminology for biorelated polymers and applications (IUPAC Recommendations 2012), Pure Appl. Chem. 84 (2) (2012) 377–410, https://doi.org/10.1351/PAC-REC-10-12-04.
[4] H.-C. Flemming, Reverse osmosis membrane biofouling, Exp. Therm. Fluid Sci. 14 (4) (1997) 382–391, https://doi.org/10.1016/S0894-1777(96)00140-9.
[5] J.S. Vrouwenvelder, D.A. Graf von der Schulenburg, J.C. Kruithof, M.L. Johns, M.C. M. van Loosdrecht, Biofouling of spiral-wound nanofiltration and reverse osmosis membranes: a feed spacer problem, Water Res. 43 (3) (2009) 583–594, https://doi.org/10.1016/j.watres.2008.11.019.
[6] Dow Water & Process Solutions, FILMTEC™ Reverse Osmosis Membranes Technical Manual.
[7] S.M. Ali, A. Qamar, S. Kerdi, S. Phuntsho, J.S. Vrouwenvelder, N. Ghaffour, H. K. Shon, Energy efficient 3D printed column type feed spacer for membrane filtration, Water Res. 164 (2019), 114961, https://doi.org/10.1016/j.watres.2019.114961.
[8] S. Kerdi, A. Qamar, A. Alpatova, J.S. Vrouwenvelder, N. Ghaffour, Membrane filtration performance enhancement and biofouling mitigation using symmetric spacers with helical filaments, Desalination 484 (2020), 114454, https://doi.org/10.1016/j.desal.2020.114454.
[9] W. Lin, Q. Wang, L. Sun, D. Wang, J. Cabrera, D. Li, L. Hu, G. Jiang, X.-m. Wang, X. Huang, The critical role of feed spacer channel porosity in membrane biofouling: insights and implications, J. Membr. Sci. 649 (2022), 120395, https://doi.org/10.1016/j.memsci.2022.120395.
[10] J.W. Koo, J.S. Ho, Y.Z. Tan, W.S. Tan, J. An, Y. Zhang, C.K. Chua, T.H. Chong, Fouling mitigation in reverse osmosis processes with 3D printed sinusoidal spacers, Water Res. 207 (2021), 117818, https://doi.org/10.1016/j.watres.2021.117818.
[11] S. Park, Y.D. Jeong, J.H. Lee, J. Kim, K. Jeong, K.H. Cho, 3D printed honeycomb-shaped feed channel spacer for membrane fouling mitigation in nanofiltration, J. Membr. Sci. 620 (2021), 118665, https://doi.org/10.1016/j.memsci.2020.118665.
[12] M.F. Nava-Ocampo, S.S. Bucs, A.S.F. Farinha, M. Son, B.E. Logan, J. S. Vrouwenvelder, Sacrificial coating development for biofouling control in membrane systems, Desalination 496 (2020), 114650, https://doi.org/10.1016/j.desal.2020.114650.
[13] A. Taiswa, J.M. Andriolo, K.R. Zodrow, J.L. Skinner, Polydopamine-copper spacers improve longevity and prevent biofouling in reverse osmosis, Water Supply 22 (10) (2022) 7782–7793, https://doi.org/10.2166/ws.2022.345.
[14] H. Sanawar, L.H. Kim, N.M. Farhat, M.C.M. van Loosdrecht, J.S. Vrouwenvelder, Periodic chemical cleaning with urea: disintegration of biofilms and reduction of key biofilm-forming bacteria from reverse osmosis membranes, Water Res. X 13 (2021), 100117, https://doi.org/10.1016/j.wroa.2021.100117.
[15] A. Siddiqui, I. Pinel, E.I. Prest, S.S. Bucs, M.C.M. van Loosdrecht, J.C. Kruithof, J. S. Vrouwenvelder, Application of DBNPA dosage for biofouling control in spiral wound membrane systems, Desalination Water Treat. 68 (2017) 12–22, https://doi.org/10.5004/dwt.2017.20370.
[16] S.R. Suwarno, X. Chen, T.H. Chong, D. McDougald, Y. Cohen, S.A. Rice, A.G. Fane, Biofouling in reverse osmosis processes: the roles of flux, crossflow velocity and concentration polarization in biofilm development, J. Membr. Sci. 467 (2014) 116–125, https://doi.org/10.1016/j.memsci.2014.04.052.
[17] S.S. Bucs, R. Valladares Linares, M.C.M. van Loosdrecht, J.C. Kruithof, J. S. Vrouwenvelder, Impact of organic nutrient load on biomass accumulation, feed channel pressure drop increase and permeate flux decline in membrane systems, Water Res. 67 (2014) 227–242, https://doi.org/10.1016/j.watres.2014.09.005.
[18] N. Derlon, P. Desmond, P.A. Rühs, E. Morgenroth, Cross flow frequency determines the physical structure and cohesion of membrane biofilms developed during gravity-driven membrane ultrafiltration of river water: implication for hydraulic resistance, J. Membr. Sci. 643 (2022), 120079, https://doi.org/10.1016/j.memsci.2021.120079.
[19] A. Seidel, M. Elimelech, Coupling between chemical and physical interactions in natural organic matter (NOM) fouling of nanofiltration membranes: implications for fouling control, J. Membr. Sci. 203 (1) (2002) 245–255, https://doi.org/10.1016/S0376-7388(02)00013-3.
[20] J.S. Vrouwenvelder, C. Hinrichs, W.G.J. Van der Meer, M.C.M. Van Loosdrecht, J. C. Kruithof, Pressure drop increase by biofilm accumulation in spiral wound RO and NF membrane systems: role of substrate concentration, flow velocity, substrate

load and flow direction, Biofouling 25 (6) (2009) 543–555, https://doi.org/10.1080/08927010902972225.
[21] P. Desmond, K.T. Huisman, H. Sanawar, N.M. Farhat, J. Traber, E.O. Fridjonsson, M.L. Johns, H.-C. Flemming, C. Picioreanu, J.S. Vrouwenvelder, Controlling the hydraulic resistance of membrane biofilms by engineering biofilm physical structure, Water Res. 210 (2022), 118031, https://doi.org/10.1016/j.watres.2021.118031.
[22] S. West, M. Wagner, C. Engelke, H. Horn, Optical coherence tomography for the in situ three-dimensional visualization and quantification of feed spacer channel fouling in reverse osmosis membrane modules, J. Membr. Sci. 498 (2016) 345–352, https://doi.org/10.1016/j.memsci.2015.09.047.
[23] C. Dreszer, H.C. Flemming, A. Zwijnenburg, J.C. Kruithof, J.S. Vrouwenvelder, Impact of biofilm accumulation on transmembrane and feed channel pressure drop: effects of crossflow velocity, feed spacer and biodegradable nutrient, Water Res. 50 (2014) 200–211, https://doi.org/10.1016/j.watres.2013.11.024.
[24] A. Siddiqui, S. Lehmann, S.S. Bucs, M. Fresquet, L. Fel, E.I.E.C. Prest, J. Ogier, C. Schellenberg, M.C.M. van Loosdrecht, J.C. Kruithof, J.S. Vrouwenvelder, Predicting the impact of feed spacer modification on biofouling by hydraulic characterization and biofouling studies in membrane fouling simulators, Water Res. 110 (2017) 281–287, https://doi.org/10.1016/j.watres.2016.12.034.
[25] J.S. Vrouwenvelder, S.A. Manolarakis, J.P. van der Hoek, J.A.M. van Paassen, W.G. J. van der Meer, J.M.C. van Agtmaal, H.D.M. Prummel, J.C. Kruithof, M.C.M. van Loosdrecht, Quantitative biofouling diagnosis in full scale nanofiltration and reverse osmosis installations, Water Res. 42 (19) (2008) 4856–4868, https://doi.org/10.1016/j.watres.2008.09.002.
[26] B. Blankert, B. Van der Bruggen, A.E. Childress, N. Ghaffour, J.S. Vrouwenvelder, Potential pitfalls in membrane fouling evaluation: merits of data representation as resistance instead of flux decline in membrane filtration, Membranes 11 (7) (2021) 460.
[27] N. Derlon, M. Peter-Varbanets, A. Scheidegger, W. Pronk, E. Morgenroth, Predation influences the structure of biofilm developed on ultrafiltration membranes, Water Res. 46 (10) (2012) 3323–3333, https://doi.org/10.1016/j.watres.2012.03.031.
[28] L. Fortunato, A. Qamar, Y. Wang, S. Jeong, T. Leiknes, In-situ assessment of biofilm formation in submerged membrane system using optical coherence tomography and computational fluid dynamics, J. Membr. Sci. 521 (2017) 84–94, https://doi.org/10.1016/j.memsci.2016.09.004.
[29] M. Wagner, D. Taherzadeh, C. Haisch, H. Horn, Investigation of the mesoscale structure and volumetric features of biofilms using optical coherence tomography, Biotechnol. Bioeng. 107 (5) (2010) 844–853, https://doi.org/10.1002/bit.22864.
[30] I.E. Idel'chik, Handbook of Hydraulic Resistance, 1960. Moscow.
[31] G. Schock, A. Miquel, Mass transfer and pressure loss in spiral wound modules, Desalination 64 (1987) 339–352.
[32] J.S. Vrouwenvelder, J.A.M. van Paassen, L.P. Wessels, A.F. van Dam, S.M. Bakker, The Membrane Fouling Simulator: a practical tool for fouling prediction and control, J. Membr. Sci. 281 (1) (2006) 316–324, https://doi.org/10.1016/j.memsci.2006.03.046.
[33] J.S. Vrouwenvelder, J.A.M. van Paassen, J.C. Kruithof, M.C.M. van Loosdrecht, Sensitive pressure drop measurements of individual lead membrane elements for accurate early biofouling detection, J. Membr. Sci. 338 (1) (2009) 92–99, https://doi.org/10.1016/j.memsci.2009.04.016.
[34] E.M.V. Hoek, J. Allred, T. Knoell, B.-H. Jeong, Modeling the effects of fouling on full-scale reverse osmosis processes, J. Membr. Sci. 314 (1) (2008) 33–49, https://doi.org/10.1016/j.memsci.2008.01.025.
[35] J.S. Vrouwenvelder, M.C.M. van Loosdrecht, J.C. Kruithof, Early warning of biofouling in spiral wound nanofiltration and reverse osmosis membranes, Desalination 265 (1) (2011) 206–212, https://doi.org/10.1016/j.desal.2010.07.053.
[36] N. Farhat, L. Kim, K. Mineta, M. Alarawi, T. Gojobori, P. Saikaly, J. Vrouwenvelder, Seawater desalination based drinking water: microbial characterization during distribution with and without residual chlorine, Water Res. 210 (2022), 117975, https://doi.org/10.1016/j.watres.2021.117975.
[37] S.S. Bucs, R. Valladares Linares, J.O. Marston, A.I. Radu, J.S. Vrouwenvelder, C. Picioreanu, Experimental and numerical characterization of the water flow in spacer-filled channels of spiral-wound membranes, Water Res. 87 (2015) 299–310, https://doi.org/10.1016/j.watres.2015.09.036.
[38] L. Fortunato, S. Bucs, R.V. Linares, C. Cali, J.S. Vrouwenvelder, T. Leiknes, Spatially-resolved in-situ quantification of biofouling using optical coherence tomography (OCT) and 3D image analysis in a spacer filled channel, J. Membr. Sci. 524 (2017) 673–681, https://doi.org/10.1016/j.memsci.2016.11.052.
[39] M. Mulder, Polarisation Phenomena and Membrane Fouling, Basic Principles of Membrane Technology, Springer Netherlands, Dordrecht, 1996, pp. 416–464, https://doi.org/10.1007/978-94-009-1766-8_7.
[40] A.R. Da Costa, A.G. Fane, D.E. Wiley, Spacer characterization and pressure drop modelling in spacer-filled channels for ultrafiltration, J. Membr. Sci. 87 (1) (1994) 79–98, https://doi.org/10.1016/0376-7388(93)E0076-.
[41] Q. She, D. Hou, J. Liu, K.H. Tan, C.Y. Tang, Effect of feed spacer induced membrane deformation on the performance of pressure retarded osmosis (PRO): implications for PRO process operation, J. Membr. Sci. 445 (2013) 170–182, https://doi.org/10.1016/j.memsci.2013.05.061.
[42] G. Pratofiorito, H. Horn, F. Saravia, Differentiating fouling on the membrane and on the spacer in low-pressure reverse-osmosis under high organic load using optical coherence tomography, Separ. Purif. Technol. 291 (2022), 120885, https://doi.org/10.1016/j.seppur.2022.120885.
[43] J. Fárková, The pressure drop in membrane module with spacers, J. Membr. Sci. 64 (1) (1991) 103–111, https://doi.org/10.1016/0376-7388(91)80081-G.
[44] V.V. Ranade, A. Kumar, Fluid dynamics of spacer filled rectangular and curvilinear channels, J. Membr. Sci. 271 (1) (2006) 1–15, https://doi.org/10.1016/j.memsci.2005.07.013.
[45] C. Picioreanu, J.S. Vrouwenvelder, M.C.M. van Loosdrecht, Three-dimensional modeling of biofouling and fluid dynamics in feed spacer channels of membrane devices, J. Membr. Sci. 345 (1) (2009) 340–354, https://doi.org/10.1016/j.memsci.2009.09.024.
[46] A.I. Radu, J.S. Vrouwenvelder, M.C.M. van Loosdrecht, C. Picioreanu, Effect of flow velocity, substrate concentration and hydraulic cleaning on biofouling of reverse osmosis feed channels, Chem. Eng. J. 188 (2012) 30–39, https://doi.org/10.1016/j.cej.2012.01.133.
[47] S. Kerdi, A. Qamar, J.S. Vrouwenvelder, N. Ghaffour, Fouling resilient perforated feed spacers for membrane filtration, Water Res. 140 (2018) 211–219, https://doi.org/10.1016/j.watres.2018.04.049.
[48] S.M. Ali, A. Qamar, S. Phuntsho, N. Ghaffour, J.S. Vrouwenvelder, H.K. Shon, Conceptual design of a dynamic turbospacer for efficient low pressure membrane filtration, Desalination 496 (2020), 114712, https://doi.org/10.1016/j.desal.2020.114712.
[49] Y. Wibisono, W. Yandi, M. Golabi, R. Nugraha, Emile R. Cornelissen, A.J. B. Kemperman, T. Ederth, K. Nijmeijer, Hydrogel-coated feed spacers in two-phase flow cleaning in spiral wound membrane elements: a novel platform for eco-friendly biofouling mitigation, Water Res. 71 (2015) 171–186, https://doi.org/10.1016/j.watres.2014.12.030.
[50] X. Liu, W. Li, T.H. Chong, A.G. Fane, Effects of spacer orientations on the cake formation during membrane fouling: quantitative analysis based on 3D OCT imaging, Water Res. 110 (2017) 1–14, https://doi.org/10.1016/j.watres.2016.12.002.
[51] A.I. Radu, J.S. Vrouwenvelder, M.C.M. van Loosdrecht, C. Picioreanu, Modeling the effect of biofilm formation on reverse osmosis performance: flux, feed channel pressure drop and solute passage, J. Membr. Sci. 365 (1) (2010) 1–15, https://doi.org/10.1016/j.memsci.2010.07.036.
[52] N.M. Farhat, M. Staal, S.S. Bucs, M.C.M. Van Loosdrecht, J.S. Vrouwenvelder, Spatial heterogeneity of biofouling under different cross-flow velocities in reverse osmosis membrane systems, J. Membr. Sci. 520 (2016) 964–971, https://doi.org/10.1016/j.memsci.2016.08.065.
[53] D.A. Graf von der Schulenburg, J.S. Vrouwenvelder, S.A. Creber, M.C.M. van Loosdrecht, M.L. Johns, Nuclear magnetic resonance microscopy studies of membrane biofouling, J. Membr. Sci. 323 (1) (2008) 37–44, https://doi.org/10.1016/j.memsci.2008.06.012.
[54] H. Horn, H. Reiff, E. Morgenroth, Simulation of growth and detachment in biofilm systems under defined hydrodynamic conditions, Biotechnol. Bioeng. 81 (5) (2003) 607–617, https://doi.org/10.1002/bit.10503.
[55] J.S. Vrouwenvelder, C. Picioreanu, J.C. Kruithof, M.C.M. van Loosdrecht, Biofouling in spiral wound membrane systems: three-dimensional CFD model based evaluation of experimental data, J. Membr. Sci. 346 (1) (2010) 71–85, https://doi.org/10.1016/j.memsci.2009.09.025.
[56] S.S. Bucs, A.I. Radu, V. Lavric, J.S. Vrouwenvelder, C. Picioreanu, Effect of different commercial feed spacers on biofouling of reverse osmosis membrane systems: a numerical study, Desalination 343 (2014) 26–37, https://doi.org/10.1016/j.desal.2013.11.007.
[57] C. Picioreanu, M.C.M. van Loosdrecht, J.J. Heijnen, Two-dimensional Model of Biofilm Detachment Caused by Internal Stress from Liquid Flow, vol. 72, 2001, pp. 205–218, https://doi.org/10.1002/1097-0290(20000120)72:2<205::Aid-bit9>3.0.Co;2-l, 2.
[58] M.G. Trulear, W.G. Characklis, Dynamics of biofilm processes, J. Water Pollut. Control Fed. 54 (9) (1982) 1288–1301.
[59] P. Stoodley, I. Dodds, J.D. Boyle, H.M. Lappin-Scott, Influence Hydrodynamics Nutrients Biofilm Struct. 85 (1998) 19S–28S, https://doi.org/10.1111/j.1365-2672.1998.tb05279.x. S1.
[60] W.G. Characklis, Bioengineering report: fouling biofilm development: a process analysis, Biotechnol. Bioeng. 23 (9) (1981) 1923–1960, https://doi.org/10.1002/bit.260230902.
[61] P.L. Bishop, J.T. Gibbs, B.E. Cunningham, Relationship between concentration and hydrodynamic boundary layers over biofilms, Environ. Technol. 18 (4) (1997) 375–385, https://doi.org/10.1080/09593331808616551.
[62] S.R. Suwarno, X. Chen, T.H. Chong, V.L. Puspitasari, D. McDougald, Y. Cohen, S. A. Rice, A.G. Fane, The impact of flux and spacers on biofilm development on reverse osmosis membranes, J. Membr. Sci. 405–406 (2012) 219–232, https://doi.org/10.1016/j.memsci.2012.03.012.